Bone and Arthrosurgery Science, 2026, Volume 4, Issue 5
https://www.bbwpublisher.com/journal/BAS
Online ISSN: 2981-8222
Print ISSN: 3083-4856

Exploratory Comparison of Three Extracorporeal Shock Wave Energy Settings and Two Transosseous Fixation Configurations in a Rabbit Rotator Cuff Repair Model: A Pilot Study

Lin Teng[1], Yue Zhang[1], Dahai Liu[1], Keyuan Ding[1], Gang Zhong[2]*

[1]Department of Orthopaedics, The First People's Hospital of Shuangliu District (West China Airport Hospital of Sichuan University), Chengdu 610200, Sichuan, China
[2]Department of Orthopedic Surgery/Trauma Center, West China Hospital, Sichuan University, Chengdu 610041, Sichuan, China

***Corresponding author:** Gang Zhong, hxzg730927@163.com

Copyright: © 2026 Author(s). This is an open-access article distributed under the terms of the Creative Commons Attribution License (CC BY 4.0), permitting distribution and reproduction in any medium, provided the original work is cited.

Abstract: *Background:* Extracorporeal shock wave therapy (ESWT) has been investigated as an adjunct to tendon-to-bone repair, but its response may vary with energy flux density and fixation configuration. Evidence concerning this possible relationship remains limited. *Methods:* This exploratory pilot study included 33 male New Zealand white rabbits. Three intact contralateral shoulders from animals in the surgery-only category served as intact reference specimens, resulting in 36 shoulder observations across eight analytical categories: intact reference, surgery-only model, and six combinations of single- or double-tunnel repair with ESWT at 0.16, 0.20, or 0.24 mJ/mm^2. Biomechanical and H&E/Masson assessments included one specimen per category. Immunohistochemistry included two specimens in each ESWT category and one specimen in each reference category; three microscopic fields were averaged within each specimen. Findings were summarized descriptively at specimen level. *Results:* Maximum loads recorded for the intact reference, surgery-only model, HS-1, HS-2, MS-1, MS-2, LS-1, and LS-2 specimens were 65, 122, 156, 178, 190, 244, 182, and 112 N, respectively. The MS-2 specimen had the highest observed value, but replication was unavailable, and load displacement curves and failure modes were not recorded. Histological material was illustrative; the LS-1 specimen showed extensive suppurative necrosis/abscess formation. TGF-β staining appeared greater in some medium-energy specimens, whereas CD34 staining varied without an interpretable specimen-level pattern. Total TGF-β and CD34 staining did not establish pathway activation or functional angiogenesis. Separately, animal Z9803 in LS-2 had mild suppuration at the surgical site on postoperative day 16. *Conclusion*: These observations generate hypotheses about possible differences among ESWT energy–fixation combinations but do not identify an optimal dose, demonstrate an energy-by-fixation interaction, or establish biomechanical efficacy, angiogenesis, or a TGF-β-mediated mechanism. A prospectively powered confirmatory study is required.

Keywords: Rotator cuff repair; Extracorporeal shock wave therapy; Tendon-to-bone healing; Pilot study; Exploratory study; Rabbit model

Online publication: November 20, 2026

1. Introduction

Rotator cuff tears are a common cause of shoulder dysfunction, particularly in older adults [1–4]. Although fixation techniques have advanced, durable recovery depends on repair at the tendon-to-bone interface, where fibrocartilage formation and collagen organization are often incomplete [1,2]. Adjunctive strategies intended to influence the local repair environment therefore remain of interest [5,6].

Extracorporeal shock wave therapy (ESWT) is a non-invasive mechanical intervention used across musculoskeletal conditions [7–9]. Experimental work has associated ESWT with changes in angiogenic and matrix-related markers, but effects depend on tissue, timing, and energy exposure [10–13]. Dose-related tissue responses have been described, including adverse changes at higher exposures in rabbit Achilles tendon [14]. Consequently, results from one energy setting cannot be assumed to define an optimum for another tissue or model.

Rotator cuff studies have already reported biomechanical, histological, and vascular observations after ESWT. Feichtinger *et al.* found improved biomechanical findings after shock wave treatment in a chronic rat repair model but did not attribute them to bone microarchitecture [15]. A subsequent rabbit study evaluated a single ESWT setting across several time points and reported changes in tendon integrity, blood perfusion, biomechanics, inflammation, and cell-related outcomes [16]. The remaining exploratory question raised by the current design is whether patterns across graded ESWT settings might differ with transosseous fixation configuration. That question requires adequate independent replication and explicit failure-mode assessment.

Accordingly, we conducted an exploratory pilot study to describe observations across three prespecified ESWT energy flux densities (0.16, 0.20, and 0.24 mJ/mm^2) and two transosseous fixation configurations in a rabbit rotator cuff repair model. The objectives were to document specimen-level biomechanical, histological, and immunohistochemical patterns and generate hypotheses for a subsequent powered study. This study was not designed to establish comparative efficacy, identify an optimal ESWT dose, test an energy-by-fixation interaction, or demonstrate a molecular mechanism.

2. Materials and methods

2.1. Study design, animals, and ethics

This was an exploratory pilot animal study. Thirty-three healthy male New Zealand white rabbits (age, 14 months; weight, 2.3–2.5 kg) were obtained from Chengdu Dashuo Experimental Animal Co., Ltd. (SCXK[Chuan]2022-039). Animals were maintained at 22 ± 2°C on a 12-h light/dark cycle with free access to food and water. The study protocol (project No. 20241226-01) was reviewed and approved by the Institutional Animal Care and Use Committee of Chengdu SenWell Experimental Animal Co., Ltd. (facility license SYXK[Chuan]2020-0232). All procedures were conducted in accordance with applicable national animal-welfare guidance.

The analysis included 33 operated shoulders (**Figure 1**). Three contralateral intact shoulders from animals in the surgery-only category were used as reference specimens, producing 36 shoulder observations but not 36 independent animals. The eight analytical categories were: intact contralateral reference (C; 3 shoulders), double-tunnel surgery-only model (M2; 3 operated shoulders), and six ESWT categories with five operated shoulders each: HS-1, HS-2, MS-1, MS-2, LS-1, and LS-2. The suffix -1 denotes single-tunnel repair and -2 denotes double-tunnel repair; HS, MS, and LS denote 0.24, 0.20, and 0.16 mJ/mm^2, respectively. Endpoint-specific specimen numbers were smaller than the category totals (**Table 1**).

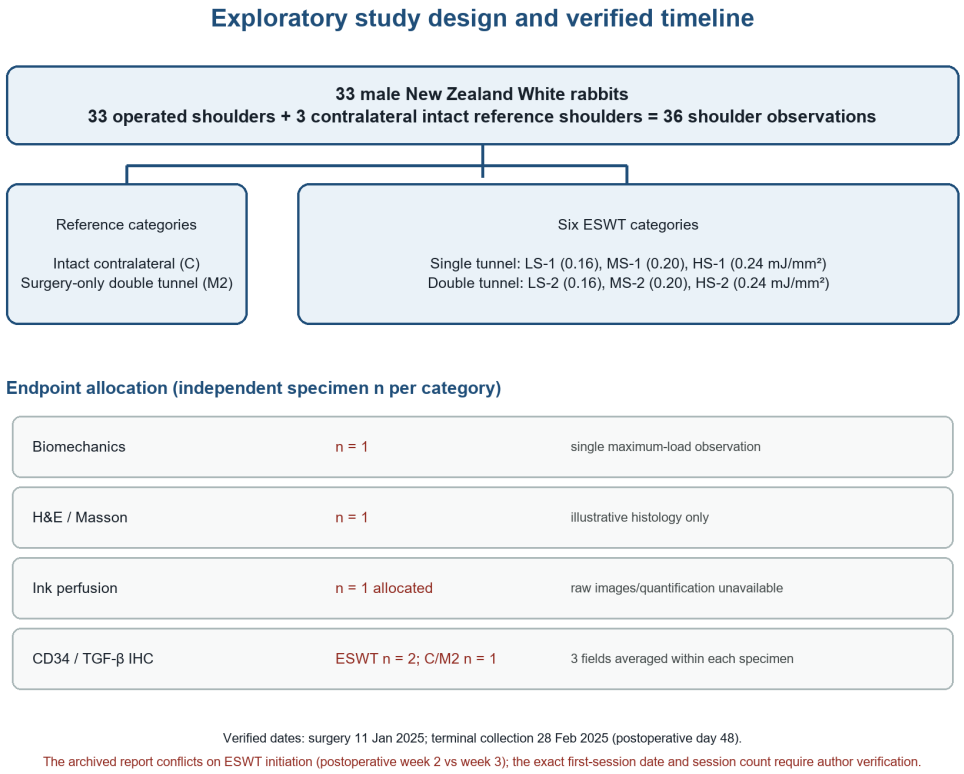


Figure 1. Exploratory study design, endpoint allocation, and available timeline. The study included 33 rabbits and 36 shoulder observations because three intact reference shoulders were contralateral shoulders rather than additional animals. The available records contain conflicting ESWT initiation references (postoperative day 14 and week 3); the exact first-session date and delivered session count could not be verified and are reported as unavailable.

Table 1. Endpoint-specific allocation. *n* denotes independent animal/shoulder specimens, not microscopic fields. Ink-perfusion specimens were allocated, but verifiable raw images and specimen-level quantitative records were unavailable for analysis.

Category	Shoulders in category	Biomechanics (*n*)	H&E/Masson (*n*)	Ink perfusion (*n*)	CD34/TGF-β (*n*)
C (intact contralateral)	3 shoulders	1	1	1 allocated	1 specimen / 3 fields
M2 (double tunnel, no ESWT)	3 shoulders	1	1	1 allocated	1 specimen / 3 fields
HS-1 (0.24, single)	5	1	1	1 allocated	2 specimens / 3 fields each
HS-2 (0.24, double)	5	1	1	1 allocated	2 specimens / 3 fields each
MS-1 (0.20, single)	5	1	1	1 allocated	2 specimens / 3 fields each
MS-2 (0.20, double)	5	1	1	1 allocated	2 specimens / 3 fields each
LS-1 (0.16, single)	5	1	1	1 allocated	2 specimens / 3 fields each
LS-2 (0.16, double)	5	1	1	1 allocated	2 specimens / 3 fields each

2.2. Surgical procedure and postoperative care

General anesthesia was induced with Zoletil. Through a longitudinal incision over the operated shoulder, the supraspinatus tendon was exposed and detached from the greater tuberosity. For repair categories, the tendon was reattached to the footprint with non-absorbable nylon sutures passed through either one oblique bone tunnel or two parallel tunnels created with a 1.0 Kirschner wire. Sutures were placed at 1.5–2-mm intervals

and tied over the tunnels. The surgery-only model used the documented double-tunnel configuration without ESWT. The incision was closed in layers. See **Figure 2**.

Perioperative care included intramuscular penicillin (60,000 U/kg twice daily for 5 days), subcutaneous meloxicam (0.1 mg/kg once daily for 3 days), and daily wound disinfection with povidone–iodine for 7 days. Animals were allowed unrestricted cage activity. Activity, appetite, wound status, behavior, coat condition, and body weight were monitored.

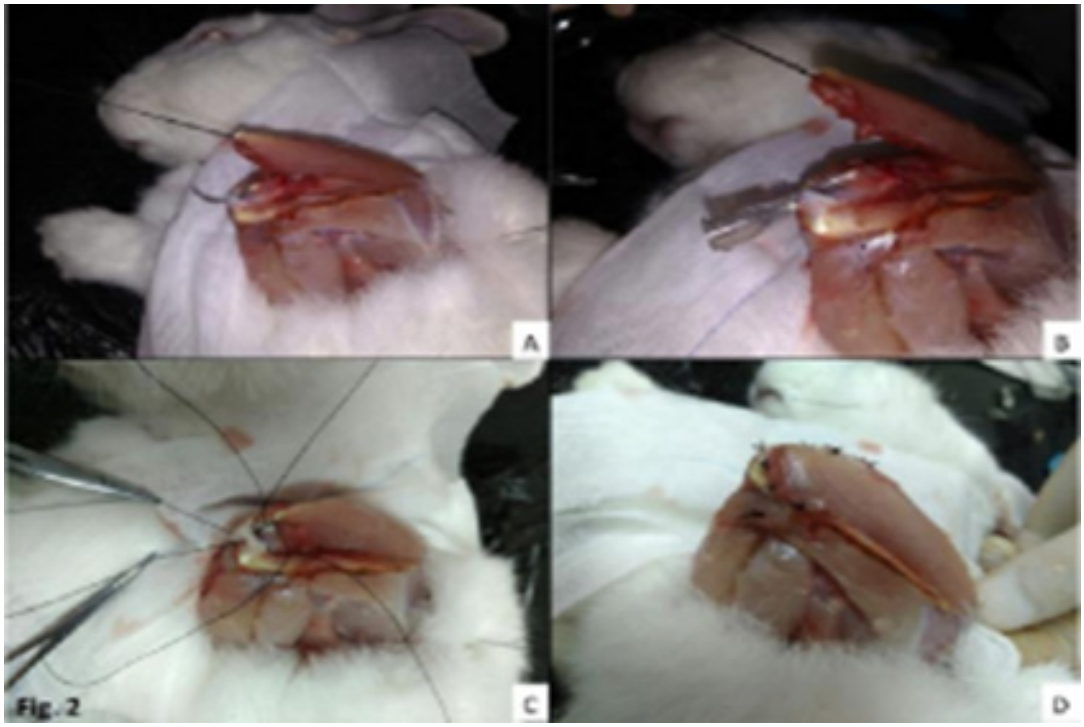


Figure 2. Surgical model and transosseous repair. (A) Supraspinatus detachment. (B) Single-tunnel repair. (C) Double-tunnel repair. (D) Tendon suturing. This figure documents construct preparation; it does not demonstrate biological healing.

2.3. ESWT protocol and study timeline

ESWT was administered with a Kartier 3621EV device to the repair footprint. Prespecified settings were 0.24 mJ/mm^2 (HS), 0.20 mJ/mm^2 (MS), and 0.16 mJ/mm^2 (LS), with 500 impulses at 4 Hz per documented session and nominal administration every 3 days for 30 days. The three settings sampled a limited prespecified range and were not intended to locate a continuous dose optimum.

Surgery was performed on 11 January 2025, and terminal collection was recorded on 28 February 2025 (postoperative day 48). The available records are inconsistent regarding ESWT initiation: one section records grouping after suture removal on postoperative day 14, whereas another states that treatment began 3 weeks after surgery. The individual treatment log was incomplete and did not permit independent verification of the first-session date or delivered session count. These parameters were therefore treated as unavailable, and no definitive treatment schedule was inferred. No claim is made that the chosen timing selectively targeted a defined healing phase.

2.4. Specimen collection and histology

At terminal collection, animals were deeply anesthetized with intramuscular Zoletil (15 mg/kg); after loss of reflexes, euthanasia was completed by intravenous pentobarbital sodium overdose (100 mg/kg) through the marginal ear vein. Supraspinatus–humerus complexes were collected. One specimen per analytical category was fixed in 10% neutral buffered formalin, decalcified, embedded in paraffin, sectioned longitudinally, and stained with hematoxylin and eosin (H&E) and Masson's trichrome.

H&E and Masson material were reviewed descriptively for tissue architecture, inflammatory changes, collagen-containing tissue, and interface continuity. Because only one specimen per category was available and section plane and region of interest were not demonstrably standardized, no group-level score or inference was made. Masson staining was not interpreted as a specific measure of collagen maturity or regenerative enthesis formation.

2.5. Ink perfusion

One specimen per analytical category was allocated to ink perfusion, with vessels to be counted in five high-power fields. However, no verifiable perfusion images or specimen-level quantitative results were available for analysis. This endpoint was therefore classified as unavailable and was not used to support vascular conclusions.

2.6. Biomechanical testing

One humerus–supraspinatus complex per analytical category was mounted in an AGX-S dual-column universal testing machine (Shimadzu, Japan), aligned with the loading axis, and loaded in uniaxial tension until failure. Maximum load (N) was recorded. Load–displacement curves, stiffness values, and failure locations were not recorded. Consequently, construct failure could not be distinguished from failure of the regenerated tendon-to-bone interface.

2.7. Immunohistochemistry

Immunohistochemistry for CD34 and total TGF-β was performed on 14 specimens: two independent specimens in each of the six ESWT categories and one specimen in each reference category. CD34 positivity was observed in endothelial, muscle, adipose, and other spindle-shaped cells; TGF-β positivity was observed in muscle, adipose, and fibrous tissue. For each marker and specimen, three fields acquired at 20× objective and 10× ocular magnification were quantified with Image-Pro Plus 6.0. Integrated optical density (IOD) and tissue area were measured, and IOD/Area was used as mean optical density. The three fields were averaged to obtain a single specimen-level value.

The laboratory reports did not provide verifiable antibody catalog numbers, dilutions, antigen-retrieval conditions, predefined region-of-interest rules, or blinding procedures. These procedural details were unavailable for retrospective verification and are treated as a methodological limitation; they were not inferred from the images.

2.8. Statistical approach

The independent experimental unit was the animal/shoulder specimen. Multiple microscopic fields from the same specimen were technical subsamples and were not treated as independent observations; the three field measurements were averaged to obtain one value per specimen. With one independent specimen per category for biomechanics and H&E/Masson histology, two specimens per ESWT category for immunohistochemistry,

and one immunohistochemical specimen per reference category, within-category variance and confirmatory between-category effects could not be estimated reliably.

Accordingly, all outcomes were presented descriptively using individual specimen values, images, and specimen-level summaries. No between-category hypothesis test, dose-response model, or interaction analysis was used, and no claim of statistical significance or optimality was made. Field-level CD34 comparisons were not retained as inferential results, because fields from the same specimen are not independent observations and therefore do not constitute animal-level evidence. No missing values were imputed.

3. Results

3.1. General observations and local adverse findings

No mortality was recorded before terminal collection. Recovery was not uniformly uneventful. On postoperative day 2, reduced food intake was recorded for Z9107 and Z9505, and an abnormal general condition was recorded for Z9307; on day 9, surgical-site fluid accumulation was recorded for Z9805. On postoperative day 16, Z9803 in LS-2 had mild suppuration at the surgical site. Z9803 later provided the LS-2 biomechanical specimen (112 N). Separately, histopathology of the LS-1 specimen Z9507 showed extensive suppurative necrosis and multiple abscess-like foci with destruction of local muscle and tendon architecture. These events are reported descriptively because the allocation did not permit estimation of complication rates or sensitivity analyses.

3.2. Exploratory biomechanical observations

Biomechanical testing was available for one specimen per analytical category (**Table 2**). Observed maximum loads ranged from 65 N in the intact contralateral specimen to 244 N in the MS-2 specimen. The lowest observed value in this series was therefore recorded in the intact contralateral reference specimen. This is not interpreted as evidence that repaired constructs exceeded native interface strength, because maximum load in a repaired shoulder reflects the combined contribution of the healing interface, the sutures, and the bone tunnels, whereas an intact tendon–bone insertion fails by a different mechanism. Because the two specimen types do not share a comparable failure mode, and given one specimen per category, the intact reference value was not compared with the repaired categories, and no inference regarding relative strength is drawn. The 244 N value was the highest among the eight tested specimens, but it was not a group mean and was not subjected to significance testing. Because load displacement curves and failure locations were unavailable, the observations cannot distinguish regenerated interface strength from suture, tunnel, or construct mechanics.

Table 2. Individual biomechanical observations. Each category contains one tested specimen; values are not group estimates. C and M2 were contralateral shoulders from the same animal (Z9207).

Category	Specimen/animal ID	Observed maximum load (N)
C	Z9207 (contralateral)	65
M2	Z9207 (operated)	122
HS-1	Z9107	156
HS-2	Z9103	178
MS-1	Z9305	190
MS-2	Z9607	244
LS-1	Z9505	182

Category	Specimen/animal ID	Observed maximum load (N)
LS-2	Z9803	112

3.3. Illustrative histological observations

H&E and Masson staining were available from one specimen per analytical category (**Figure 3**). The displayed sections differed in anatomical composition and section plane. Some sampled medium-energy sections contained comparatively aligned collagen-rich tissue, while sampled high-energy sections showed edema and inflammatory changes. The LS-1 specimen showed extensive suppurative necrosis/abscess formation. These appearances are illustrative and cannot establish category-level differences in collagen density, maturity, fibrocartilage regeneration, or tendon-to-bone integration. Masson-positive collagen could include regenerative tissue, fibrotic scar, or both.

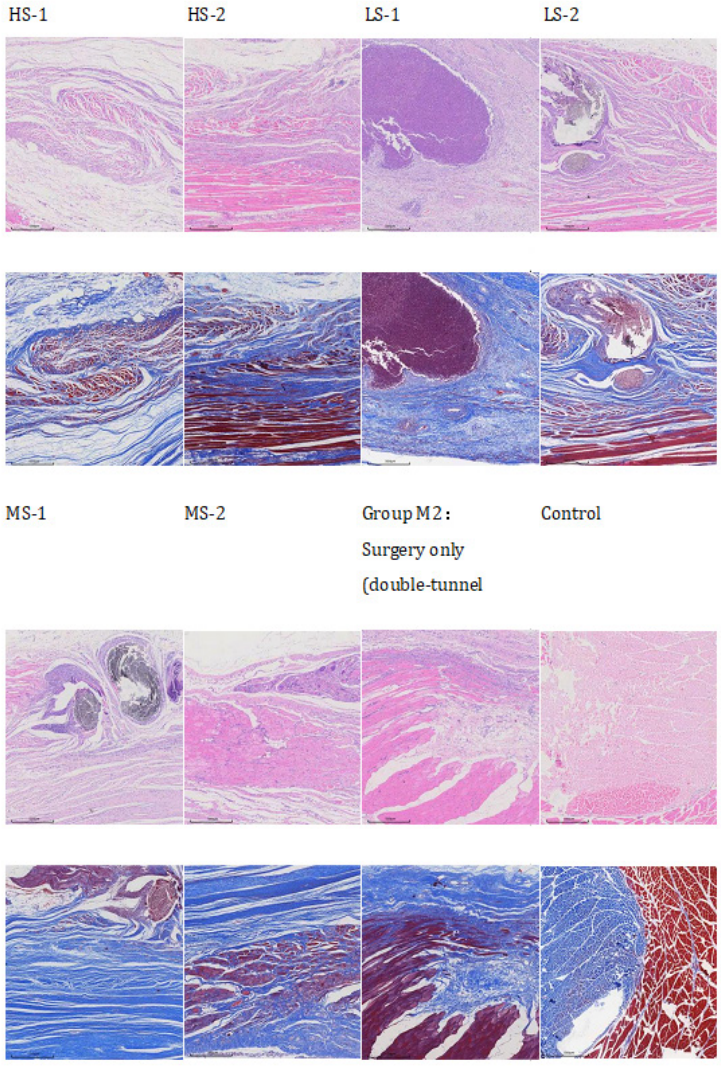


Figure 3. Illustrative H&E and Masson fields from the single available specimen in each analytical category. The first and third rows show H&E; the second and fourth rows show Masson staining. Scale bars = 500 μm. The LS-1 specimen contains an abscess/suppurative lesion. Owing to one specimen per category and non-standardized section composition, the panels do not constitute a group-level comparison of collagen maturity or interface regeneration.

3.4. CD34 immunoreactivity

CD34 immunoreactivity was detected across the sampled specimens (**Figure 4**). Specimen-level IOD/Area values, after averaging three fields within each specimen, were: C 0.0186 (n = 1), M2 0.0294 (n = 1), HS-1 0.0241 and 0.0258, HS-2 0.0301 and 0.0536, MS-1 0.0282 and 0.0349, MS-2 0.0363 and 0.0374, LS-1 0.0378 and 0.0484, and LS-2 0.0266 and 0.0369. The small and unequal numbers of independent specimens did not support a confirmatory category-level comparison. CD34 staining at a single terminal time point did not demonstrate vessel patency, tissue perfusion, or the timing of angiogenesis.

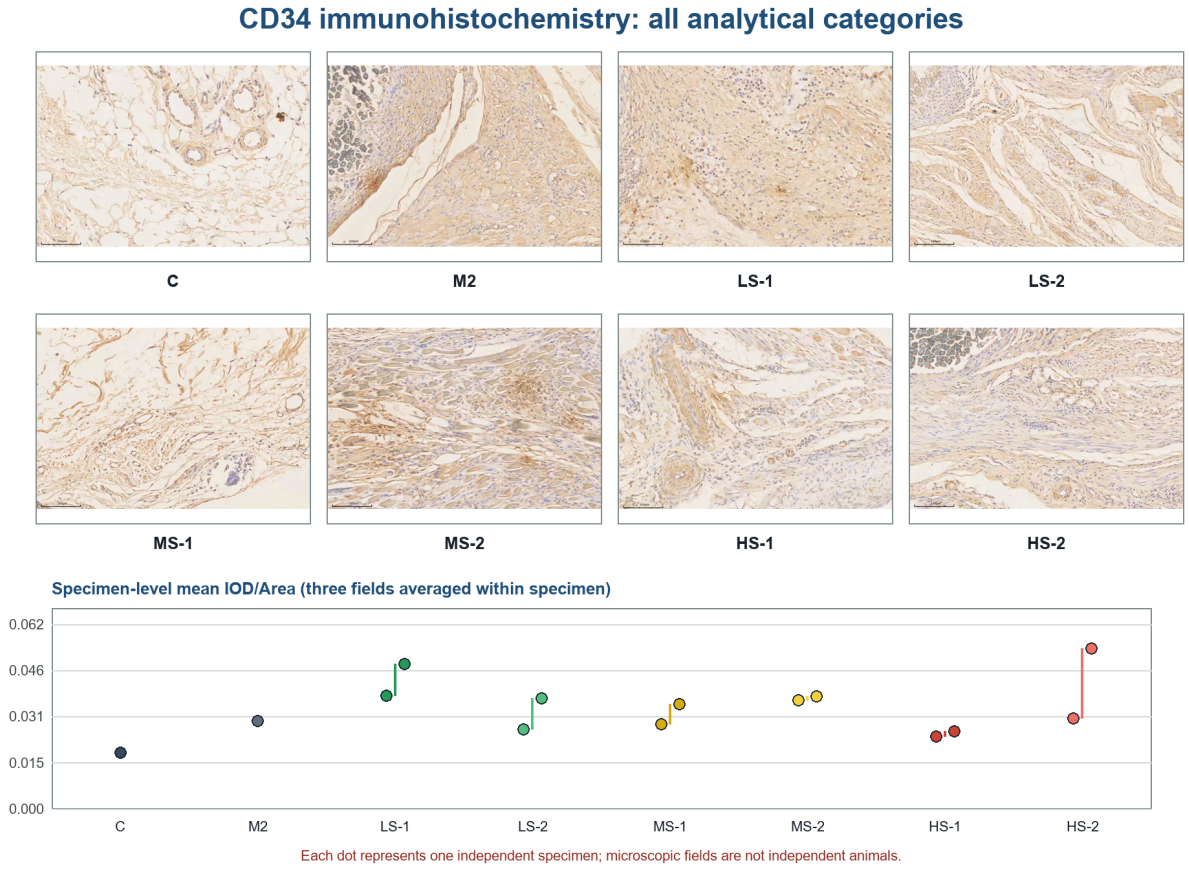


Figure 4. CD34 immunohistochemistry across all eight analytical categories. Images are illustrative fields from the first archived specimen in each category (scale bars embedded in source images = 100 µm). The lower panel shows specimen-level mean IOD/Area after averaging three fields within each specimen. Each dot is one independent specimen; fields are technical subsamples. ESWT categories included two specimens each; C and M2 included one specimen each. No inferential comparison was performed.

3.5. Total TGF-β immunoreactivity

Total TGF-β immunoreactivity varied among specimens (**Figure 5**). Specimen-level IOD/Area values were (**Table 3**): C 0.00945 (n = 1), M2 0.00939 (n = 1), HS-1 0.00538 and 0.00462, HS-2 0.01456 and 0.01064, MS-1 0.05402 and 0.02588, MS-2 0.05199 and 0.02410, LS-1 0.01049 and 0.02079, and LS-2 0.00816 and 0.01922. Some medium-energy specimens had higher observed values than several other specimens, but batch-to-batch variation and sparse independent replication precluded confirmatory inference. Total TGF-β immunoreactivity did not establish active TGF-β/SMAD signaling and did not distinguish regenerative

remodeling from fibrosis or scar formation.

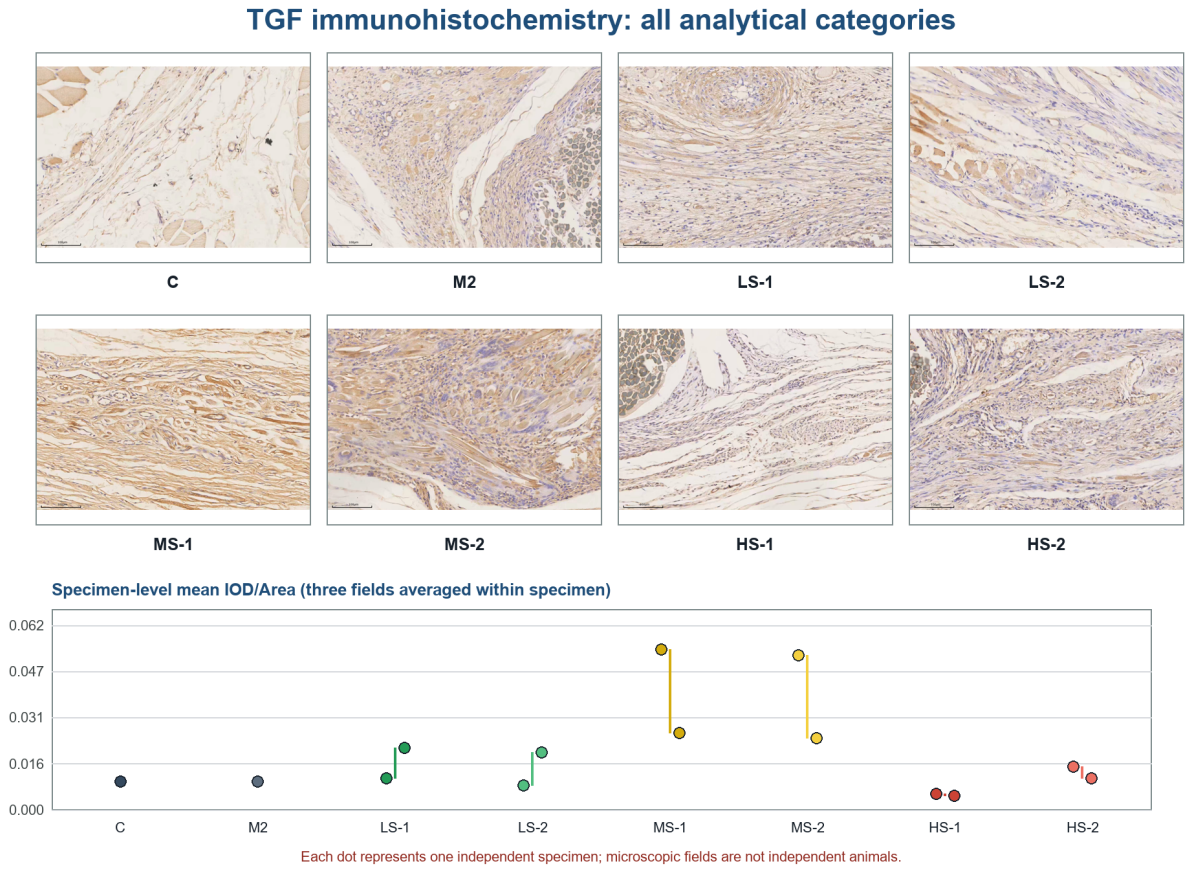


Figure 5. Total TGF-β immunohistochemistry across all eight analytical categories. Images are illustrative fields from the first archived specimen in each category (scale bars embedded in source images = 100 µm). The lower panel shows specimen-level mean IOD/Area after averaging three fields within each specimen. Each dot is one independent specimen; no *P*-values are reported because independent replication was insufficient for confirmatory inference.

Table 3. Specimen-level IOD/Area means for CD34 and total TGF-β after averaging three microscopic fields within each specimen. Specimen 1 and specimen 2 correspond to the two archived batches when available; a dash indicates that only one reference specimen was available. Values are descriptive and are not group estimates.

Category	CD34 specimen 1	CD34 specimen 2	TGF-β specimen 1	TGF-β specimen 2
C	0.018612	—	0.009448	—
M2	0.029384	—	0.009388	—
HS-1	0.024107	0.025821	0.005385	0.004623
HS-2	0.030121	0.053608	0.014555	0.010635
MS-1	0.028232	0.034936	0.054022	0.025877
MS-2	0.036319	0.037428	0.051992	0.024098
LS-1	0.037759	0.048388	0.010493	0.020787
LS-2	0.026581	0.036923	0.008163	0.019220

4. Discussion

This pilot study generated three main specimen-level observations. First, the single MS-2 specimen had the highest maximum load among the eight specimens tested. Second, some medium-energy sections contained comparatively organized collagen-rich tissue in the displayed histology. Third, some medium-energy specimens showed greater total TGF-β staining. These observations raise a hypothesis that ESWT energy and fixation configuration might jointly influence the repair environment. Their apparent agreement, however, is not replicated evidence of efficacy, an optimal energy setting, or an energy-by-fixation interaction.

The biomechanical observations require particular caution. Each category contributed only one specimen. The constructs used non-absorbable sutures, and tunnel number may directly alter load distribution and initial fixation strength. Because load displacement curves, stiffness, and failure sites were not recorded, the 244 N observation in MS-2 cannot be attributed specifically to tendon-to-bone regeneration. It may reflect biological variation, technical variation, construct geometry, or a combination of these factors. The individual values can inform the design of later testing but cannot establish superiority.

The histological material also provides illustrative rather than comparative evidence. With one specimen per category and possible differences in section level and tissue composition, apparent differences in collagen alignment, edema, and inflammatory tissue cannot be generalized. Masson staining identifies collagen-containing tissue but does not establish collagen maturity or distinguish organized enthesis regeneration from fibrotic scar. Future confirmatory work would require standardized harvesting, a prespecified region of interest, blinded scoring, and independent animal replication.

The immunohistochemical findings do not establish a mechanism. Total TGF-β immunoreactivity may accompany matrix remodeling, but it may also occur with fibrosis and myofibroblast activity. Demonstrating a TGF-β-mediated regenerative pathway would require active ligand, downstream signaling such as phosphorylated SMAD2/3, relevant matrix targets, and ideally pathway perturbation. The present pattern is therefore an association for follow-up. Similarly, CD34 staining did not show a stable specimen-level pattern and was measured at only one terminal time point. CD34 immunoreactivity cannot demonstrate that new vessels were patent or perfused. The unavailable ink-perfusion data further prevent functional vascular interpretation.

The local suppurative findings are important. Extensive suppurative necrosis occurred in the examined LS-1 histological specimen, while Z9803 in LS-2 had mild surgical-site suppuration and later contributed to the 112 N load observation. These events indicate that postoperative recovery was not uniformly uneventful and may have influenced local tissue and mechanical outcomes. With the present endpoint allocation, complication incidence and its relationship to energy or fixation cannot be estimated.

Prior animal studies have already examined ESWT in rotator cuff repair using biomechanical, histological, vascular, and molecular outcomes [15,16]. The distinctive hypothesis suggested by this design is whether response to graded ESWT differs according to fixation configuration. This pilot dataset cannot test that interaction. Its contribution is limited to feasibility information, transparent documentation of individual observations, and identification of design requirements for later work. No recommendation about clinical ESWT dose, indication, postoperative timing, or rehabilitation can be derived.

4.1. Limitations

Endpoint-specific independent sample sizes were extremely small: biomechanics and H&E/Masson histology

included one specimen per category; immunohistochemistry included two specimens per ESWT category and one specimen per reference category.

Microscopic fields were technical subsamples within specimens; treating fields as independent animals would be pseudoreplication.

The three intact reference shoulders were contralateral shoulders, so 36 shoulder observations did not represent 36 independent rabbits.

The available records contain conflicting ESWT initiation references (postoperative day 14 vs week 3), and the first-session date and delivered session count could not be independently verified.

Biomechanical curves, stiffness, and failure modes were unavailable, preventing separation of construct mechanics from biological healing.

Histological sampling and regions of interest were not standardized sufficiently for group comparison; Masson staining did not specifically measure collagen maturity.

Ink-perfusion results were unavailable; terminal CD34 staining did not establish functional or early neovascularization.

Total TGF-β staining did not establish signaling activation or causality, and staining-batch effects may have contributed to variation.

Local suppurative events may have influenced outcomes, and the sparse allocation precluded sensitivity analyses.

Only three closely spaced energy settings were sampled; even a replicated difference would not by itself locate a continuous-dose optimum.

5. Conclusion

In this exploratory rabbit study, the highest maximum load was observed in a single specimen treated with 0.20 mJ/mm^2 ESWT and double-tunnel repair, and some medium-energy specimens showed comparatively organized histological features and greater total TGF-β staining. Owing to sparse independent replication and limitations of the available endpoints, these observations do not demonstrate treatment efficacy, an optimal energy, an energy-by-fixation interaction, functional angiogenesis, or a TGF-β-mediated mechanism. The data may assist the design of a future powered study but do not support clinical recommendations.

Acknowledgments

The authors thank the laboratory staff of Sichuan Yanxt Technology Co., Ltd. for technical assistance with histological sectioning and immunohistochemical analysis.

Funding

This study was supported by the Science and Technology Projects of Xizang Autonomous Region, China (Grant No. XZ202501ZY0112), the Medical Research Project of Chengdu Municipal Health Commission (Grant No. 2023131), and the Science and Technology Assistance Program of Sichuan Provincial Department of Science and Technology (Grant No. 2024YFHZ0124).

Disclosure statement

The authors declare no conflict of interest.

References

[1] Bedi A, Bishop J, Keener J, et al., 2024, Rotator Cuff Tears. Nature Reviews Disease Primers, 10(1): 8.

[2] Lapner P, Henry P, Athwal GS, et al., 2022, Treatment of Rotator Cuff Tears: A Systematic Review and Meta-Analysis. Journal of Shoulder and Elbow Surgery, 31(3): e120–e129.

[3] Murrell G, Walton JR, 2001, Diagnosis of Rotator Cuff Tears. The Lancet, 357(9258): 769–770.

[4] Sambandam SN, Khanna V, Gul A, et al., 2015, Rotator Cuff Tears: An Evidence Based Approach. World Journal of Orthopedics, 6(11): 902.

[5] Pasculli RM, Bowers RL, 2022, Evidence-Based Management of Rotator Cuff Tears (Acute and Chronic). Current Physical Medicine and Rehabilitation Reports, 10(3): 239–247.

[6] Trygonis N, Loupasis T, Hautz WE, et al., 2026, Conservative Management of Degenerative Rotator Cuff Tears: A Systematic Review of Long-Term Clinical Outcomes and Cost Effectiveness. Journal of Orthopaedics, 75: 232–241.

[7] De la Corte-Rodríguez H, Román-Belmonte JM, Rodríguez-Damiani BA, et al., 2023, Extracorporeal Shock Wave Therapy for the Treatment of Musculoskeletal Pain: A Narrative Review. Healthcare, 11(21): 2830.

[8] Rhim HC, Shin J, Kang J, et al., 2024, Use of Extracorporeal Shockwave Therapies for Athletes and Physically Active Individuals: A Systematic Review. British Journal of Sports Medicine, 58(3): 154–163.

[9] Zhang X, Ma Y, 2023, Global Trends in Research on Extracorporeal Shock Wave Therapy (ESWT) from 2000 to 2021. BMC Musculoskeletal Disorders, 24(1): 312.

[10] Sugiyama T, Murakami H, Tanaka S, et al., 2025, Effects of Extracorporeal Shockwave Therapy on Wound Healing in Rats. Cureus, 17(5): e83369.

[11] Sung PH, Yeh JN, Yin TC, et al., 2025, Extracorporeal Shockwave Therapy Rescued Mouse Critical Limb Ischemia Via Upregulating GPR120 Against Inflammation and Promoting Angiogenesis for Restoring the Blood Flow in Ischemic Zone-Experimental Study. International Journal of Surgery, 111(3): 2414–2429.

[12] Sung PH, Yin TC, Chai HT, et al., 2022, Extracorporeal Shock Wave Therapy Salvages Critical Limb Ischemia in B6 Mice through Upregulating Cell Proliferation Signaling and Angiogenesis. Biomedicines, 10(1): 117.

[13] Abbas A, Khan Z, Veqar Z, 2023, Dose Dependent Effects of Extracorporeal Shockwave Therapy on Pain and Function in Osteonecrosis of Femoral Head: A Systematic Review. Journal of Clinical Orthopaedics and Trauma, 45: 102275.

[14] Rompe JD, Kirkpatrick CJ, Kullmer K, et al., 1998, Dose-Related Effects of Shock Waves on Rabbit Tendo Achillis. A Sonographic and Histological Study. J Bone Joint Surg Br, 80(3): 546–552.

[15] Feichtinger X, Heimel P, Tangl S, et al., 2022, Improved Biomechanics in Experimental Chronic Rotator Cuff Repair After Shockwaves Is Not Reflected by Bone Microarchitecture. PLoS One, 17: e0262294.

[16] Wang H, Wu F, Miao JQ, 2026, Effects of Extracorporeal Shock Wave Therapy on Tendon Integrity, Biomechanical Strength, Matrix Remodeling, Inflammation, Angiogenesis, and Tenogenic Differentiation in Rotator Cuff Injury. Kaohsiung J Med Sci, 2026: e70260.

Publisher's note

Bio-Byword Scientific Publishing remains neutral with regard to jurisdictional claims in published maps and institutional affiliations.